AC electroosmosis micromixing on a lab-on-a-foil electric microfluidic device

Mengren Wu, Yuan Gao, Amirreza Ghaznavi, Weiqi Zhao, and Jie Xu

Department of Mechanical and Industrial Engineering, University of Illinois at Chicago, Chicago, IL 60607, USA

Highlights

- Flexible electric lab-on-a-foil devices are fabricated using plastic and electrode films.
- Local pattern of AC electroosmotic flow mixing was quantitively studied on microfluidic chip.
- The relative mixing index (RMI) of micromixing achieves higher than 0.9.
- RBCs aggregation was successfully fabricated with continuous flow.

Abstract

Efficient mixing of fluids in lab-on-a-chip devices is very important for many biomedical and biochemical applications. Lab-on-a-foil as a novel concept provides a method for fast prototyping or mass production of microfluidic device based on thin and flexible films materials. In this article, electroosmosis micromixing is conducted in a lab-on-a-foil microfluidic device. With the electroosmotic flow (EOF), an efficient micromixing is realized inside a microchannel by tooth-shaped planar electrodes. The mixing performance is evaluated based on intensity measurement, and frequency sweeping is used to identify optimal performance. Furthermore, according to local intensity profiles, the EOF pattern is analyzed to provide a deep understanding on the influence of frequency and flow rate. The amplitude of voltage and the number of pairs of electrode tooth are also investigated to find the optimal conditions of the device. To the best of our knowledge, this is the first demonstration of the AC EOF in a lab-on-a-foil electric device and the exploration of EOF pattern vertically and horizontally in the microchannels. This study provides a method to optimize mixing performance in EOF-based micromixer. Furthermore, the fabrication method cast the potential to mass production of low-cost flexible electric microfluidic device.

Keywords: Lab-on-a-foil, Micromixing, AC electroosmosis, RBCs aggregation

Acknowledgements

This work was supported by the National Science Foundation (No. 1917295).

1. Introduction

Microfluidics serves as an effective platform for manipulating fluids for scientific and industrial applications in a variety of fields such as analytical chemistry, biochemical analysis, and biomedical sciences [1]. A multi-functional miniaturized microfluidic device, or so-called lab-on-a-chip, integrates several laboratory functions on a tiny chip. In the past two decades, microfluidic devices have become one of the main applications of microfabrication technology in biomedical and biochemical science due to the capability of precisely handling minute amounts of biological liquid quickly and efficiently. While benefiting from the advantages of miniaturization such as low volume, energy consumption, low-cost, and portability, microfluidics technology also faces new challenges owing to counter-intuitive fluid physics at microscale. Since the Reynolds number of liquid flows in the microchannel is typically very low (<<1), fluids mixing is mainly achieved by diffusion, which is an inefficient and inherently slow process. To address this issue, many types of micromixers [2-4] have been developed for various microfluidic applications in recent years, which are categorized into passive and active mixers.

Microfluidic devices have been advanced for extended functionalities by integrated modalities with external energy including acoustic, optical, magnetic, and electrical energy. Among these energy types, electrical energy is a good candidate for scaling down. Since the electric field becomes more dominant when the operating scale is reduced, it has been widely applied in microfluidic devices. Driven by electrical energy, one of the electrokinetic phenomena, electroosmotic flow [5-8], occurs in porous materials, capillary tubes or microchannels. Since chemical equilibrium between liquid and solid surface leads to surface charge distributions, the liquid interface acquires a net fixed electrical charge. When an electric field is applied to the fluid, the charge will be driven by electrical potential gradients and thus EOF will be created [9]. Recently, AC electroosmotic flow (AC-EOF) has been studied experimentally and theoretically by applying an AC voltage to the electrodes in a microfluidic channel. Depending on the configuration of electrodes, the electric field direction and effect vary within microfluidic channels. For example, Modarres et al. used a three-finger sinusoidally shaped electrode to generate electroosmotic flow across the fluid stream's direction to investigate the impact of AC voltage on the mixing in a microchannel [10]. Ren et al. theoretically studied a pair of sharp electrodes induced electroosmosis for a mixing application [11]. Huang et al. applied various configurations of electrodes to generate EOF with in-plane microvortices for effective mixing in the microchannel [12]. Sasaki et al. studied meandering electrodes configured in parallel to the microchannel for chemical processing [13]. However, the complex fabrication processes for the electric microfluidic device limit the comprehensive study of the influence of electrode configuration on the AC EOF performance.

Electrode fabrication in electric microfluidic devices is commonly based on metal film deposition using a lift-off process [14]. As to the fabrication of microfluidic channels, soft lithography techniques have been widely used combining with the PDMS replica techniques [15, 16]. These fabrication processes usually require large foot-print equipments and long operation time. Therefore, these processes are not suitable for fast prototyping or mass production for the related study and applications. Recently, a novel concept of lab-on-a-foil has emerged in the microfluidics field. Different from PDMS-based microfluidic devices, lab-on-a-foil system is constructed by thin and flexible films, which enable high volume production of disposable, flexible and low-cost chips. At present, various methods have been applied in fabrication of lab-on-a-foil devices including micro-thermoforming [17], hot roller embossing [18], dry resist technologies [19] laser micromachining [20], and xurography [21]. Among these methods, xurography is a simple and flexible technique with the help of a digital plotter to fabricate microfluidic channels on thin film materials. The cut films are then bonded layer by layer to enclose flow paths, and the off-the-shelf film materials are usually used, such as biocompatible adhesive tapes [22] and thermoplastic films [23].

In our group's previous work, an acoustic micromixer has been successfully integrated into the lab-on-a-foil system [24]. However, since the acoustic micromixer needs to integrate with a rigid piezoelectric transducer to connect the energy source, it makes the device still not flexible for the real mixing applications. Different from our previous work, we present an innovative method by applying xurography to create flexible electrodes, microfluidic channels and assembling them to a lab-on-a-foil electric microfluidic device. Taking the advantages of rapid and simple fabrication, we comprehensively investigated the electrokinetic phenomenon, AC EOF, in lab-on-a-foil electric microfluidic devices. It worth to note that in this work we not only simplified the microelectrodes array fabrication but also deeply studied the AC EOF local pattern during the mixing process, which may benefit for future wearable mixing applications.

Herein, we provide a novel method for the study of AC electroosmosis micromixing in a lab-on-a-foil electric microfluidic device. In this work, using xurography technique, a pair of tooth-shaped electrodes is integrated with a microfluidic channel by control of an AC power source. To validate the electric field in the microfluidic channel, numerical simulation is conducted with the same configuration of experimental setup (Supplementary Figure S1). By applying an AC source with different frequencies, the mixing performance of two parallel flow streams in various flow rates is analyzed by relative mixing index (RMI). In addition, the EOF mixing pattern is quantitively studied for a better understanding of mixing process in local position. The impact of the voltage, flow rate and the number of pairs of electrode tooth on the mixing performance is investigated and evaluated for various potential chemical and biological applications. The RBC aggregation with the continuous flow is successfully performed using this device. To the best of our knowledge, this is the first-time demonstration of the AC EOF in a lab-on-a-foil device with an exploration of EOF local pattern. This work not only provides a method to optimize mixing performance in EOF-based micromixer but also casts the potential for mass production of low-cost flexible electric microfluidic device.

2. Material and methods

a. AC-EOF mixing mechanism

The working mechanism of AC electroosmosis mixer is shown in figure 1. The proposed micromixer consists of a T-shaped microchannel with two inlets and one outlet. In this T-shaped microchannel, a pair of tooth-shaped electrodes were placed on two side walls to generate AC-EOF. The tooth-shaped electrodes were designed with several pairs of electrode tooth vertically and staggeringly aligned with flow streaming in the microchannel. Figure 1a) shows the schematic diagram of electrode configuration and AC-EOF across the microchannel. The AC-EOF mixing is generated when the electric field was applied to the device. Specifically, by staggeringly aligning two electrodes around the straight microchannel, the AC-EOF is perpendicular with the laminar flow direction in microchannel. When AC-EOF occurs between each pair of electrodes tooth, it facilitated the mass transport across the channel to perturb the laminar flow driven by liquid motion exerted on the electrical double layer of electrodes in the channel achieving a rapid mixing of two reagents. Thus, two fluid streams mix while flowing toward the same outlet. The mixing of two different agents in this device are fluorescent dye and deionized (DI) water, which is shown in figure 1 b). In addition, to demonstrate the mixing effect for mixing sample with particles, the fluorescent polymer beads and DI water are employed, which is shown in Figure 1c). To understand the impact of AC power on mixing effect, the frequency and voltage sweeping were performed on this device. In addition, the same device configuration was used to investigate impact of the EOF pattern and tooth number.

b. AC-EOF theory background

The AC-EOF is driven by liquid motion exerted on the electrical double layer by a tangential electric field [10, 25]. When the planar microelectrode is immersed in an electrolytic medium, the electrode polarization occurs, which is the process that ions migrate to the surface of the electrode and neutralize the charge from the electrode to induce an electrical double layer [25-27]. By the planar microelectrodes, the divergent electric field is induced. As a result, a component of electric field tangentially lies on a diffuse double layer is created on the electrode surface. Thus, the diffuse double layer experiences a time-averaged force [5] of that acts from edge-to-edge crossing the surface of electrodes. However, the double layer becomes more complex in the AC electric field compared to the situation in the DC electric field described by Debye [26, 28]. The ions in solution respond to the charge on the electrode at each half-cycle and are retarded by frictional drag through the liquid. With the AC electric field, electrode charge oscillates faster than the response of ions, which leads to an incomplete formation of a diffuse double layer. As a result, the electrode polarization and AC-EOF will be weaker at higher frequencies. The time-averaged electroosmotic velocity at distance x from inner electrode spacing can be expressed by this equation [10],

$$v = \frac{1}{2} Re\left\{\frac{\Delta\sigma_q E_x^*}{\mu K}\right\} = \frac{1}{8}\frac{\varepsilon V^2 \Omega^2}{\mu x(1+\Omega^2)^2}\frac{C_s}{C_s + C_d} \tag{1}$$

$$\Omega = \omega \frac{\varepsilon}{\sigma}\frac{\pi}{2} xK \tag{2}$$

where ε is the permittivity, σ is the conductivity, and μ is the viscosity of liquid. V is the amplitude of AC power source, K^{-1} is the Debye length of the double layer, ω is the angular frequency, and Ω is the non-dimensional characteristic frequency. $\Delta\sigma_q$ is the time-dependent excess charge in the diffuse layer and E_x^* is the tangential electric field component. $\frac{C_s}{C_s+C_d}$ represents a correction factor with C_s being the Stern layer (or compact layer) capacitance and C_d being the diffuse layer capacitance.

c. Fabrication process

The lab-on-a-foil device consists of a top layer, channel layer, bottom layer and electrode layer. A double-sided adhesive tape (ARcare® 90445, Adhesives Research, Glen Rock, PA) which is a transparent medical grade tape with good biocompatibility and aqueous insolubility, was used for fabricating the top, channel and bottom layers [29-31]. A double conductive copper adhesive tape (Zehhe Copper Foil Tape with Double-Sided Conductive) was used for constructing the electrode layer. The xurography technique was applied on the thin film material using a desktop digital cutting plotter (QuicKutz Silhouette SD, QuicKutz, Inc.) to fabricate designed patterns (figure 2a). To assemble all layers, the protective liner of each layer was peeled off and an alignment tool composed of a three-axis linear stage was applied to carefully align all layers under a microscope (Supplementary Figure S2). Two branch microchannels (800 µm in width, 200 µm in depth) and one outlet was designed and fabricated with the same dimension. The tooth-like electrode was designed with different numbers of pairs of electrode tooth (800 µm in width) and the distance from each other was 1.1 mm. Afterwards, two electrodes were oppositely and staggeringly placed on two sides of the microchannel, which is shown in figure 2b.

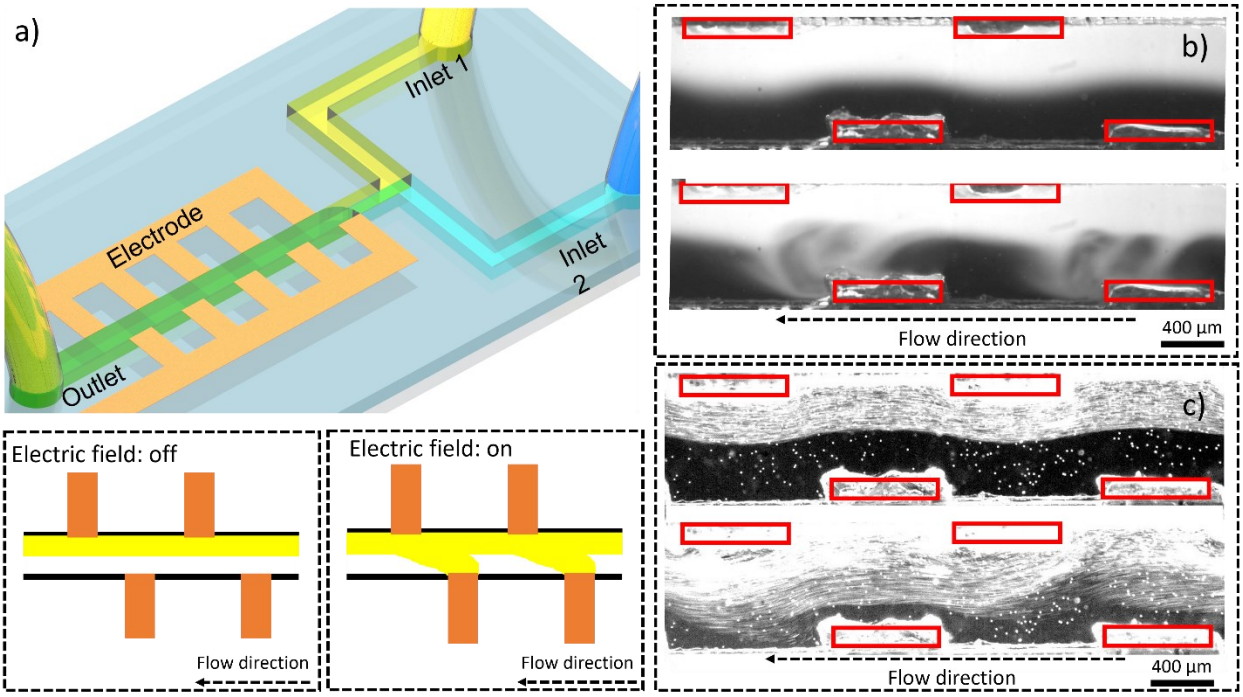

Figure 1. Schematic illustration of AC electroosmosis micromixing. a) Overview of device and working mechanism; b) Mixing of DI water with fluorescent dye; c) Mixing of DI water with fluorescent particles.

d. Experimental setup

To evaluate the mixing effect, the DI water and fluorescent dye solution (Fluorescein sodium salt, Sigma-Aldrich, St. Louis) were pumped in two inlets by using two syringe pumps (FUSION 200, Chemyx Inc). The PDMS was punched into two inlets using a puncher with the diameter of 2 mm. The distance between two inlets was same with the ones of the device. To assemble the PDMS connector with the device, adhesive layer was revealed after the protection linear of top layer of the device was peeled off. During the assembly process, the two inlets of the PDMS connector were aligned with the two inlets of the device. After that, the PDMS connector was bond with the adhesive layer of the top layer of the lab-on-a-foil device. The tube was connected to a PDMS connector bonded on the lab-on-a-foil device [32] The device was mounted on an inverted microscope system (Nikon Eclipse Ti–S, Nikon Instruments Inc.). Moreover, DI water and fluorescent particles were also applied to this device to demonstrate the performance of particle mixing. The fluorescent dye and particles were excited using a fluorescence illuminator (X-cite 120, Lumen Dynamics, Ontario, Canada), and the intensity was captured using a high-speed camera (Phantom Miro M310, Vision Research Inc., USA). Then, a waveform generator (DG1022U; Rigol Technologies Inc., Beijing, China) was connected with the electrode layer to generate sine wave signals. The signals were amplified by a voltage amplifier (Tegam 2350, Tegam Inc., Madison, OH). The driving frequency was set from 1Hz to 1MHz, and the driving voltage was applied from 0.5 Vpp to 1 Vpp to evaluate mixing performance.

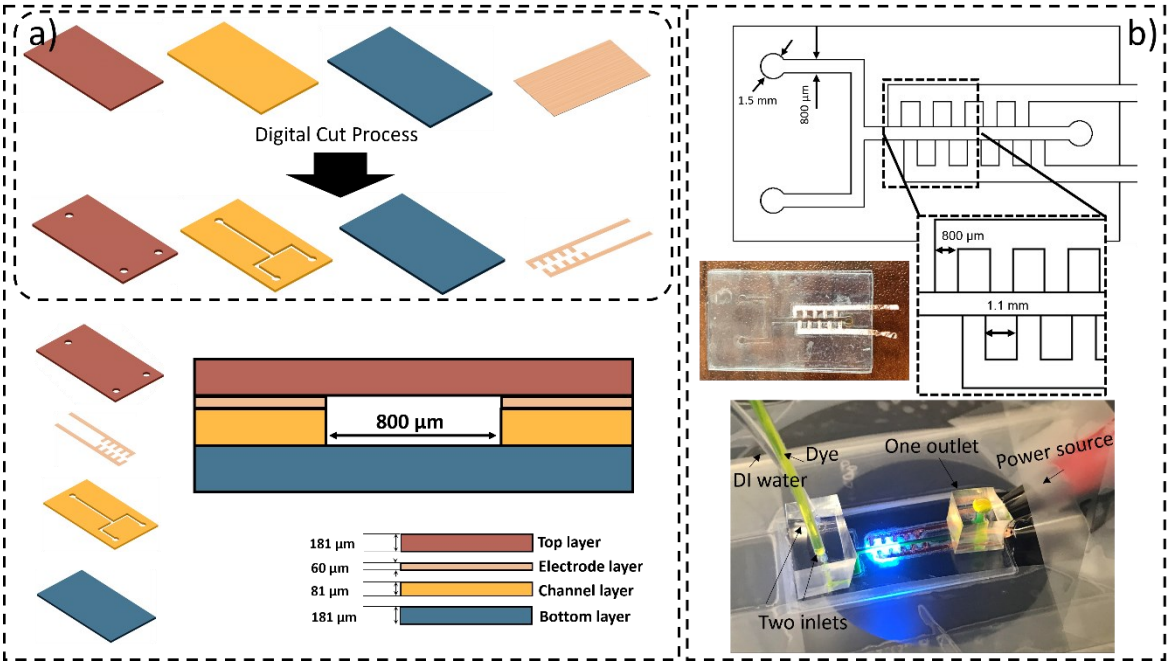

Figure 2. Schematic illustration of fabrication and experimental setup a) Digital plotter cut process for each layer, and diagram of side view of device. b) Dimension of device and images of experimental setup.

3. Results and discussion

a. Effect of driving frequency

To investigate the effect of mixing with various frequencies and flow rates, the signal frequency was swept in a range from 1 Hz to 1 MHz with a step that is 10 times the previous one. For each frequency, the total flow rates 15, 20, 25, and 30 µl/min were performed in this experiment to study the impact of flow rate on effect performance. It is worth noting that the flow rate mentioned here refers the total flow rate in the microchannel, which is the sum of the flow rate of the two inlets and the flow rates from each inlet is same. In addition, to better understand the mixing effect of each pair of electrode tooth in local position,

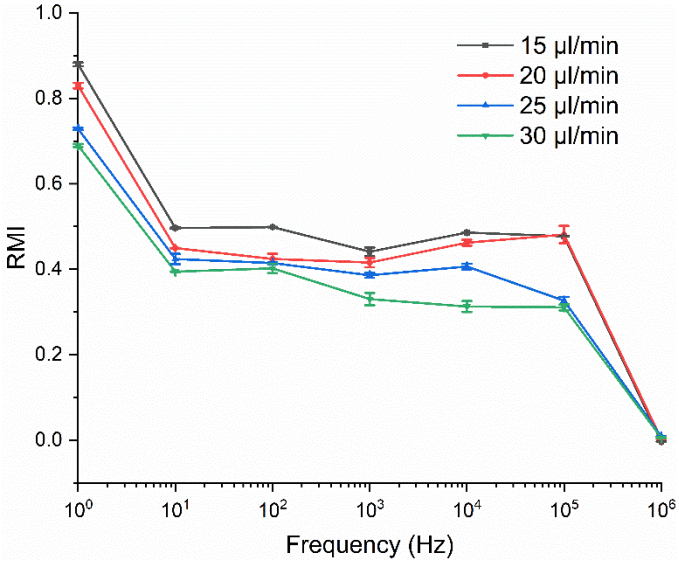

Figure 3. Plot of mixing perfomance versus driving frequency.

we further quantitively analyzed the intensity distribution and pattern across the microchannel with different flow rates.

To quantitatively characterize the performance of mixing, a relative mixing index was calculated based on the microscope image sequence. Different from absolute mixing index, RMI includes initial conditions of each experiment and precludes the influence of lighting conditions [33]. The standard deviation of the pixel intensities in two conditions (σ mixed and σ_o unmixed) are involved to calculated according to the formula as follows:

$$RMI = 1 - \frac{\sigma}{\sigma_o} = 1 - \frac{\sqrt{\frac{1}{N}\sum_{i=1}^{N}(I_i - \langle I \rangle)^2}}{\sqrt{\frac{1}{N}\sum_{i=1}^{N}(I_{oi} - \langle I \rangle)^2}}$$

where I_i, I_{oi}, $\langle I \rangle$ show a local pixel intensity, a local pixel intensity in the unmixed case, and the average of the pixel intensities in the region of interest, respectively. N represents the total number of pixels. In this process, the ROI (200*150 pixels) at the outlet was selected and analyzed before and after the mixing process in the same position of the channel, which is shown in Figure 3. The standard deviation and mean value of grayscale intensity in the ROI were measured using ImageJ. After calculation, the results in Figure 3 indicated that at 1 Hz frequency of AC electric field, the optimal mixing performance occurs in four different flow rates. However, the mixing performance decreased because of the increasing flow rate of fluid in the microchannel. In this situation, the effect of EOF becomes weaker and intensity distribution in local position is changed with various flow rates. When frequency was set from 10 Hz to $1x10^5$ Hz, the optimum performance was achieved at 15 µl/min at 10 Hz (RMI=0.49), while the lowest (RMI=0.31) occurs when the flow rate is 30 µl/min at $1x10^5$ Hz. At the frequency of $1x10^6$ Hz, the RMI of four different flow rates dropped to around zero. It is worth noting that the viscosity of fluid is a factor affecting the mixing performance. Previous works have numerically and experimentally studied the viscosity of biofluid in EOF [34, 35]. Based on time-averaged velocity equation, the velocity of EOF inversely proportional to the viscosity, which causes different mixing effects.

b. EOF pattern analysis

To further understand the EOF between two electrode edges and the impact of flowrate on EOF pattern, the distribution of fluorescent dye was analyzed using grayscale intensity in local position. The selection of region of interest (ROI) and measurement of intensity were conducted using an open-source software ImageJ.

As aforementioned in theory background, in each half-cycle of AC signal, the mixing effect is generated by EOF when the ions in solution respond to the charge on the electrode. Figure 4(a) shows the diagram of local EOF pattern at different flow rates of agents. During the first half-cycle, the 1st EOF occurs at first pair (1-a,1-b) and the mixed liquid flows with the streaming to outlet. Afterwards, at the beginning of second half-cycle of signal, the 2nd EOF occurs at the second pair of electrode tooth (2-a, b). At the moment of mixed fluid passing second pair of electrode tooth, two different mixing patterns occur in this device depends on the flow rate of sample: 1) At lower flow rate, the second EOF (2nd in figure) occurs before the first mixed liquid (1st in figure) arriving the second pair of electrode tooth (2-a, b); 2) At higher flow rate, the second EOF (2nd in figure) occurs after the first mixed liquid (1st in figure) arriving the second pair of electrode tooth (2-a, b). These phenomena significantly impact mixing performance with same frequency of signal from the intensity analysis.

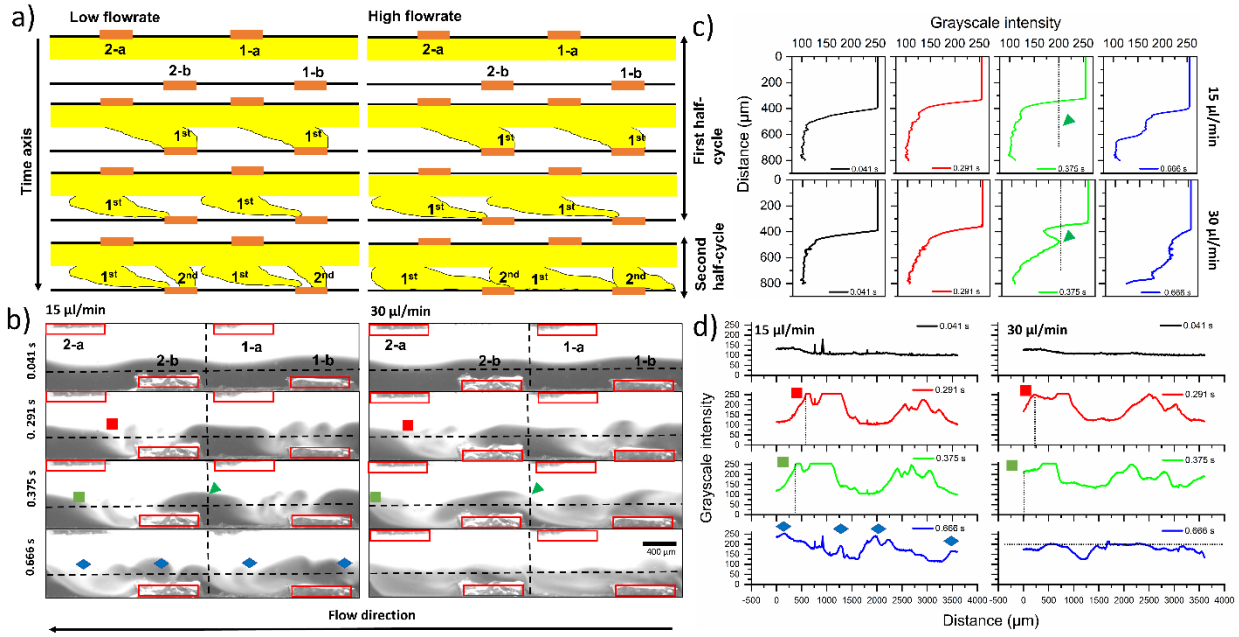

Figure 4. AC EOF local pattern analysis a) Schematic illustration of the EOF pattern in a lower and higher flowrate. The first three rows show the first EOF occurs in first half-cycle. The last row shows two different patterns in second half-cycle. b) Image sequence at 0.041 s, 0.291 s, 0.375 s, and 0.666 s. The dash lines in figures show intensity analysis in vertical and horizontal position. c) Vertical intensity analysis results showing first mixed liquid were detected at 0.375 s at 30 μl/min. d) Horizontal intensity analysis results show that during the second half-cycle (0.666s), four intensity peaks occur in 15 μl/min.

The microscope image sequence at flow rate of 15 μl/min and 30 μl/min were analyzed to quantitively compare the relationship of first mixed liquid position and second mixed liquid pattern. It is worth noting that, first half cycle to second half cycle was analyzed since the intensity pattern during this period is distinct without any overlap and influence from previous mixing effect. Figure 4 (b) shows the images captured at 0.041, 0.291, 0.375 and 0.666 s after AC electric field was applied. The vertical (0 to 800 μm) and horizontal line (0 to 3600 μm) was set to measure intensity changed along with the line at different times. The vertical line is set between the two pairs of electrode tooth to quantify the position of the mixed liquid after the first EOF. The results in figure 4 (c) show that intensity of DI water agent flow (400 μm to 800 μm) was enhanced at 0.666 s with 15 μl/min flow rate. However, the intensity of the same position in 30 μl/min enhanced at 0.375 s. Since the AC applied in this process is a sine signal with 1 Hz, the second half-cycle takes place at 0.5 second. With applying this AC power source, the second EOF came out at 0.5 s while first mixed liquid passed at 0.666 s and 0.375 s in 15 μl/min and 30 μl/min flow rate, respectively. In a higher flow rate mixing, the first EOF local pattern has an overlap area with the second electrode and the second EOF occurs on mixed liquid. When the flow rate is 15 ul/min, the two kinds of unmixed fluid have been mixed four times, while at the 30 ul/min, the two kinds of unmixed fluid were mixed twice, and then the mixed fluid was mixed twice at the same condition.

To validate this phenomenon, the horizontal line was set in DI water phase and close to the interface of two agents. According to the intensity profile along with horizontal line, the homogenous intensity at the 0.041 s and two peaks at 0.291s and 0.375 s show EOF was triggered and crossing the microchannel in both flowrates. In the intensity profile of 15 μl/min flow, the first peak appears in the 500 μm at 0.291 s and 300 μm at 0.375 s. Different from the 15 μl/min, the first peak occurs at 250 μm and around 100 μm at same time at 30 μl/min flow. This result is highly consistent with the vertical intensity analysis and validate mixed liquid pattern at same frequency in different flow rates. The previous analysis results show

that at 1 Hz, the mixing effect is better at 15 µl/min than 30 µl/min. Such experimental results also can be inferred from horizontal intensity analysis at 0.666s which is 0.16s later than 2nd EOF (0.5 s). Figure 4 d) shows that four intensity peaks appeared in the flow of 15 µl/min, but the intensity is homogeneous in the flow of 30 µl/min. It is worth noting that this homogeneous intensity is lower than the four peaks. Because of the slow flow, the two EOFs generated four times of mixing in the two pairs of electrode tooth. However, in the fast flow, the second EOF overlapped with the first EOF, which leads to a weakening of the mixing effect. This result has a great agreement with RMI measurements at the outlets of microchannel.

c. Effect of driving voltage

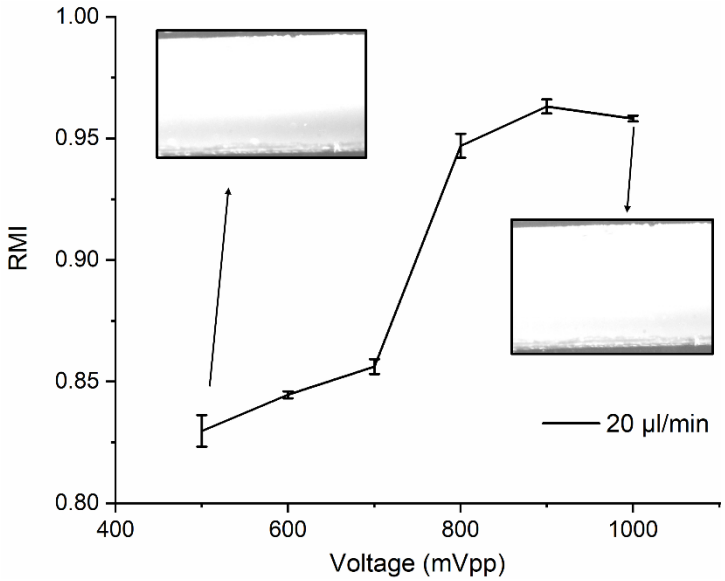

Figure 5. Plot of mixing perfomance versus driving voltage at 20µl/min flow rate, illustrating the area of ROI at 500 mVpp and 1000 mVpp.

Except for the frequency of AC power source, the amplitude of power is another vital parameter for mixing performance. To further characterize the mixing behavior, we applied 1 Hz input voltage from 500 mVpp to 1000 mVpp with a 100 mVpp increment to actuate AC EOF mixing at 20 ml/min. All data were obtained with same ROI area (200*150 pixels) at outlet of channel. As shown in Figure 5, when the voltage ranges from 700 mVpp to 800 mVpp, the mixing performance increases significantly and achieves around 0.95. These experimental results are reasonable because electroosmosis velocity is proportional to the second power of the amplitude of power. The microscope image captured in outlet also indicates mixed liquid tends to uniform from an amplitude of 800 mVpp to 1000 mVpp.

d. Effect of tooth number

In this part, we investigated the relationship between the number of pairs of electrode tooth and mixing performance at various flow rates 15, 20, 25 and 30 µl/min. The electrodes with 1, 3, and 5 pairs of electrode tooth were fabricated and assembly to lab-on-a-foil device. To ensure that all experiments were conducted under the same conditions, the distance between the ROI and the last electrode in each device was designed to be same. In addition, the same driving frequency 1 Hz was applied during the experiment. As shown in Figure 6, the mixing performance in four flow rates increases with increment of number of electrodes.

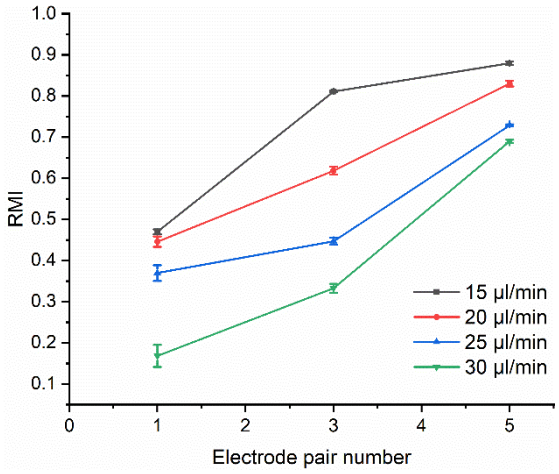

Figure 6. Plot of mixing perfomance versus electrode pair number at four different flow rates.

In a lower flow rate 15 µl/min, the increment of pair number caused a dramatic increase in mixing performance from 1 pair to 3 pairs of electrode tooth. On the contrary, at a higher flow rate, the rate of increase on mixing performance becomes slow. This phenomenon has a great agreement with the EOF pattern analysis because at a lower flow rate, there is no overlap between first and second EOF flow. On the other hand, from 3 to 5 pairs, its rate of increasing is lower than others since the performance at the 3 pair is best among four flow rates and closes to performance at 5 pairs of electrode tooth.

e. Application of AC-EOF micro mixing

To assess the applicability of the AC-EOF micromixing in biofluid applications, the generation of red blood cells aggregation was conducted in proposed lab-on-a-foil electric platform. Since RBCs aggregation is a major determinant of in vitro rheological properties of blood and occurred in several diseases associated with vascular disorders, the aggregation of red blood cells by protein or polymer attracts biophysical interest [36]. In previous studies, the red blood cells (RBCs) aggregation model was studied by mixing RBCs with dextran solution [36-38]. When RBCs

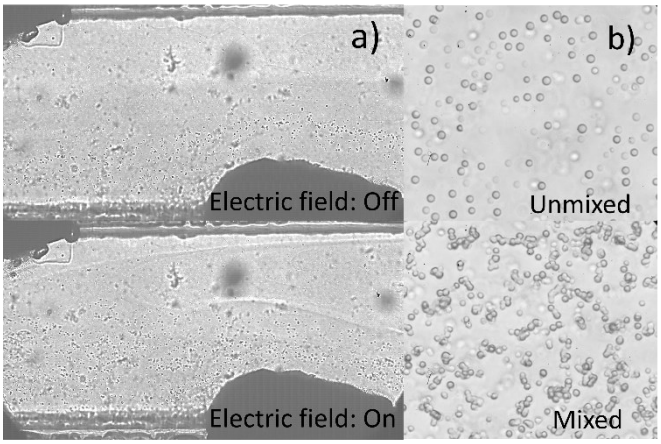

Figure7. RBCs aggregation generation process a) The whole blood sample and dextran-PBS were mixed between electrodes b) Unmixed blood sample and RBCs aggregation after mixing

aggregation flows in narrow microchannel, it is affected by a significantly increased shear force and were broken [39], which affects the study of the RBC aggregation. Using this device, the generation of RBCs aggregation with a continuous flow was conducted in this mixing platform, which minimizes the shear force of injection process. Porcine whole blood from Innovative Research Inc. was used in this demonstration. The blood sample was diluted by PBS buffer solution, which is consist of 6.25% blood + 93.75% 1× PBS solution. The dextran used in this experiment is Dx 500 and was diluted by 1× PBS solution with a weight ratio of 2.5 g per 100 ml [37]. The blood sample and dextran-PBS solution were injected into this device at total flow rate 15 µl/min. When driving voltage of 900 mV with 1 Hz applied to the device, two fluids was mixed in this device and mixed sample was collected at the outlet. The whole blood sample before and after mixing was shown in figure 7. The results show that the electric microfluidic platform successfully mixed the blood sample with dextran solution and fabricated RBC aggregates with continuous flow at flow rate 15 µl/min. This demonstration also proved the biocompatibility of proposed electric microfluidic platform.

4. Conclusion

In this work, an AC EOF micromixing in a lab-on-a-foil microfluidic device was demonstrated. The microfluidic device was fabricated by xurography using flexible material. In this process, the biocompatible double-sided tape and copper film were cut using a digital plotter and assembly layer by layer which provides a low-cost, mass production method. Based on the control of power source and flow rate of two streaming, we investigated the impact of frequency on mixing performance with different flow rates. At 1 Hz, the mixing performance was the best in 15, 20, 25, and 30 µl/min streaming. In addition, the mixing performance decreased with the increase of flow rate. To qualify the detail of mixing phenomena, we measured the EOF intensity pattern in local position between two electrodes vertically and horizontally. After electric field was applied on the device, according to the intensity pattern along with the horizontal line, the first EOF extended to the second pair of electrodes faster in higher flow rate than in lower flow rate. This is the reason causing an additional mixing of two unmixed agents and higher performance of mixing in a lower flow rate. Also, to valid this situation, the horizontal intensity pattern was measured to deliver interface pattern of two agents. The results are highly consistent with the vertical intensity analysis which shows four intensity peaks appear in the flow of 15 µl/min and the intensity is homogeneous in the flow of 30 µl/min. In addition, the mixing performance was evaluated under the different driving voltages and number of pairs of electrode tooth. The results show the mixing performance increases when the amplitude of voltage and number of pairs of electrode tooth is increased. To the best of our knowledge, this is the first-time demonstration of the AC EOF in a lab-on-a-foil device and exploration of EOF pattern vertically and horizontally in the microchannels. This study provides a method to optimize mixing performance in EOF-based micromixer. Furthermore, the fabrication method cast the potential to massive produce low-cost flexible microfluidic mixers.

Reference

1. Whitesides, G.M., *The origins and the future of microfluidics.* nature, 2006. **442**(7101): p. 368-373.
2. Hessel, V., H. Löwe, and F. Schönfeld, *Micromixers—a review on passive and active mixing principles.* Chemical engineering science, 2005. **60**(8-9): p. 2479-2501.
3. Cai, G., et al., *A review on micromixers.* Micromachines, 2017. **8**(9): p. 274.
4. Bayareh, M., M.N. Ashani, and A. Usefian, *Active and passive micromixers: A comprehensive review.* Chemical Engineering and Processing-Process Intensification, 2020. **147**: p. 107771.

5. Ramos, A., et al., *Ac electrokinetics: a review of forces in microelectrode structures.* Journal of Physics D: Applied Physics, 1998. **31**(18): p. 2338.
6. Ramos, A., et al., *Pumping of liquids with ac voltages applied to asymmetric pairs of microelectrodes.* Physical review E, 2003. **67**(5): p. 056302.
7. Wiley, D. and G. Fimbres Weihs, *Electroosmosis.* Encyclopedia of Membranes. Springer Berlin Heidelberg, Berlin, Heidelberg, 2015. **10**: p. 978-3.
8. Xuan, X. and D. Li, *Electroosmotic flow in microchannels with arbitrary geometry and arbitrary distribution of wall charge.* Journal of colloid and interface science, 2005. **289**(1): p. 291-303.
9. Marina, M.L. and M. Torre, *Capillary electrophoresis.* Talanta, 1994. **41**(9): p. 1411-1433.
10. Modarres, P. and M. Tabrizian, *Phase-controlled field-effect micromixing using AC electroosmosis.* Microsystems & Nanoengineering, 2020. **6**(1): p. 1-11.
11. Ren, Y., et al., *On ac-field-induced nonlinear electroosmosis next to the sharp corner-field-singularity of leaky dielectric blocks and its application in on-chip micro-mixing.* Micromachines, 2018. **9**(3): p. 102.
12. Huang, S.-H., et al., *AC electroosmotic generated in-plane microvortices for stationary or continuous fluid mixing.* Sensors and Actuators B: Chemical, 2007. **125**(1): p. 326-336.
13. Sasaki, N., T. Kitamori, and H.-B. Kim, *AC electroosmotic micromixer for chemical processing in a microchannel.* Lab on a Chip, 2006. **6**(4): p. 550-554.
14. Čemažar, J., D. Miklavčič, and T. Kotnik, *Microfluidic devices for manipulation, modification and characterization of biological cells in electric fields–a review.* J. Microelectron. Electron. Compon. Mater, 2013. **43**: p. 143-161.
15. Whitesides, G.M., et al., *Soft lithography in biology and biochemistry.* Annual review of biomedical engineering, 2001. **3**(1): p. 335-373.
16. Xia, Y. and G.M. Whitesides, *Soft lithography.* Annual review of materials science, 1998. **28**(1): p. 153-184.
17. Truckenmüller, R., et al., *Flexible fluidic microchips based on thermoformed and locally modified thin polymer films.* Lab on a Chip, 2008. **8**(9): p. 1570-1579.
18. Li, J., et al., *Hot embossing/bonding of a poly (ethylene terephthalate)(PET) microfluidic chip.* Journal of Micromechanics and Microengineering, 2007. **18**(1): p. 015008.
19. Focke, M., et al., *Lab-on-a-Foil: microfluidics on thin and flexible films.* Lab on a Chip, 2010. **10**(11): p. 1365-1386.
20. Malek, C.K., L. Robert, and R. Salut, *Femtosecond laser machining and lamination for large-area flexible organic microfluidic chips.* The European Physical Journal-Applied Physics, 2009. **46**(1).
21. Bartholomeusz, D.A., R.W. Boutté, and J.D. Andrade, *Xurography: rapid prototyping of microstructures using a cutting plotter.* Journal of Microelectromechanical systems, 2005. **14**(6): p. 1364-1374.
22. Yuen, P.K. and V.N. Goral, *Low-cost rapid prototyping of flexible microfluidic devices using a desktop digital craft cutter.* Lab on a Chip, 2010. **10**(3): p. 384-387.
23. Shaegh, S.A.M., et al., *Plug-and-play microvalve and micropump for rapid integration with microfluidic chips.* Microfluidics and Nanofluidics, 2015. **19**(3): p. 557-564.
24. Lin, Y., et al., *Acoustofluidic micromixer on lab-on-a-foil devices.* Sensors and Actuators B: Chemical, 2019. **287**: p. 312-319.
25. Green, N.G., et al., *Fluid flow induced by nonuniform ac electric fields in electrolytes on microelectrodes. I. Experimental measurements.* Physical review E, 2000. **61**(4): p. 4011.
26. Scott, M., K.V. Kaler, and R. Paul, *Theoretical model of electrode polarization and AC electroosmotic fluid flow in planar electrode arrays*. 2001, Elsevier.

27. Castellanos, A., et al. *AC electric-field-induced fluid flow in microelectrode structures: scaling laws*. in *Proceedings of 2002 IEEE 14th International Conference on Dielectric Liquids. ICDL 2002 (Cat. No. 02CH37319)*. 2002. IEEE.
28. Debye, P. and E. Hückel, *De la theorie des electrolytes. I. abaissement du point de congelation et phenomenes associes.* Physikalische Zeitschrift, 1923. **24**(9): p. 185-206.
29. Patko, D., et al., *Microfluidic channels laser-cut in thin double-sided tapes: Cost-effective biocompatible fluidics in minutes from design to final integration with optical biochips.* Sensors and Actuators B: Chemical, 2014. **196**: p. 352-356.
30. Eletxigerra, U., J. Martinez-Perdiguero, and S. Merino, *Disposable microfluidic immuno-biochip for rapid electrochemical detection of tumor necrosis factor alpha biomarker.* Sensors and Actuators B: Chemical, 2015. **221**: p. 1406-1411.
31. Santiago-Felipe, S., et al., *Real-time loop-mediated isothermal DNA amplification in compact disc micro-reactors.* Biosensors and Bioelectronics, 2016. **79**: p. 300-306.
32. Mohanty, S., D. Beebe, and G. Mensing, *PDMS connectors for macro to microfluidic interfacing. Chips & Tips.* Lab on a Chip, 2006. **23**.
33. Hashmi, A. and J. Xu, *On the quantification of mixing in microfluidics.* Journal of laboratory automation, 2014. **19**(5): p. 488-491.
34. Hadigol, M., et al., *Numerical study of electroosmotic micromixing of non-Newtonian fluids.* Journal of Non-Newtonian Fluid Mechanics, 2011. **166**(17-18): p. 965-971.
35. Mukherjee, S., et al., *Electroosmosis of viscoelastic fluids: Role of wall depletion layer.* Langmuir, 2017. **33**(43): p. 12046-12055.
36. Neu, B., R. Wenby, and H.J. Meiselman, *Effects of dextran molecular weight on red blood cell aggregation.* Biophysical journal, 2008. **95**(6): p. 3059-3065.
37. Xu, X., et al., *Effect of dextran-induced changes in refractive index and aggregation on optical properties of whole blood.* Physics in Medicine & Biology, 2003. **48**(9): p. 1205.
38. Buxbaum, K., E. Evans, and D. Brooks, *Quantitation of surface affinities of red blood cells in dextran solutions and plasma.* Biochemistry, 1982. **21**(13): p. 3235-3239.
39. Kang, Y.J., *Periodic and simultaneous quantification of blood viscosity and red blood cell aggregation using a microfluidic platform under in-vitro closed-loop circulation.* Biomicrofluidics, 2018. **12**(2): p. 024116.